Inorg. Chem. **2008**, *47*, 78–93

Epoxidation and 1,2-Dihydroxylation of Alkenes by a Nonheme Iron Model System – DFT Supports the Mechanism Proposed by Experiment

Peter Comba* and Gopalan Rajaraman

Universität Heidelberg, Anorganisch-Chemisches Institut, INF 270, D-69120 Heidelberg, Germany

Received June 14, 2007

The Fe^{II} complexes of two isomeric pentadentate bispidine ligands in the presence of H_2O_2 are catalytically active for the epoxidation and 1,2-dihydroxylation of cyclooctene (bispidine = 3,7-diazabicyclo[3.3.1]nonane; the two isomeric pentadentate bispidine ligands discussed here have two tertiary amine and three pyridine donors). The published spectroscopic and mechanistic data, which include an extensive set of ^{18}O labeling experiments, suggest that the Fe^{IV}═O complex is the catalytically active species, which produces epoxide as well as *cis*- and *trans*-1,2-dihydroxylated products. Several observations from the published experimental study are addressed with hybrid density functional methods and, in general, the calculations support the proposed, for nonheme iron model systems novel mechanism, where the formation of a radical intermediate emerges from the reaction of the Fe^{IV}═O oxidant and cyclooctene. The calculations suggest that the $S = 1$ ground state of the Fe^{IV}═O complex reacts with cyclooctene in a stepwise reaction, leading to the formation of a carbon-based radical intermediate. This radical is captured by O_2 from air to produce the majority of the epoxide products in an aerobic atmosphere. Under anaerobic conditions, the produced epoxide product is due to the cyclization of the radical intermediate. Several possible spin states ($S_T = 3, 2, 1, 0$) of the radical intermediate are close in energy. As a result of the substantial energy barrier, calculated for the $S_T = 3$ spin ground state, a spin-crossover during the cyclization step is assumed, and a possible two-state scenario is found, where the $S = 2$ state of the Fe^{IV}═O complex participates in the catalytic mechanism. The 1,2-dihydroxylation proceeds, as suggested by experiment, via an unprecedented pathway, where the radical intermediate is captured by a hydroxyl radical, the source of which is Fe^{III}—OOH, and this reaction is barrierless. The calculations suggest that dihydroxylation can also occur by a direct oxidation pathway from Fe^{III}—OOH. The strikingly different reactivities observed with the two isomeric bispidine Fe^{II} complexes are rationalized on the basis of structural and electronic differences.

Introduction

In the past decade, the Fe^{IV}═O group has attracted much attention in bioinorganic chemistry and catalysis. Complexes with an Fe^{IV}═O center are active in various biomolecules such as cytochrome P450, bleomycin, phenylalanine hydroxylase, and α-ketoglutarate dependent enzymes (α-KG).[1] Many of these biomolecules have a heme ferryl group, but nonheme Fe^{IV}═O-based active sites are also known. The well-characterized heme enzyme cytochrome P450 is known to catalyze a variety of reactions such as oxidation, reduction, isomerization, and dehydration. Evidence for reactive nonheme Fe^{IV}═O groups has been found for the α-KG dioxygenase TauD.[2] Several synthetic nonheme model complexes have been prepared, and their catalytic properties have been explored.[3] Mechanistic studies of heme and nonheme model complexes are of interest as these are expected to shed light on the complex biological processes and will also help to design new catalysts with increasing efficiency and selectivity.

The electronic structure of heme and nonheme ferryl complexes has been under intense spectroscopic and theoretical study.[1,4–19] Stable Fe^{IV}═O complexes have been produced and characterized spectroscopically,[20] and two

* To whom correspondence should be addressed. E-mail: peter.comba@aci.uni-heidelberg.de. Phone: +49-6221-548453. Fax: +49-6226-548453.

(1) (a) Solomon, E. I.; Brunold, T. C.; Davis, M. I.; Kensley, J. N.; Lee, S.-K.; Lehnert, N.; Neese, F.; Skulan, A. J.; Yang, Y.-S.; Zhou, J. *Chem. Rev.* **2000**, *100*, 235. (b) Nam, W. *Acc. Chem. Res.* **2007**, *40*, 522.

(2) Price, J. C.; Barr, E. W.; Tirupati, B.; Bollinger, Jr., M.; Krebs, C. *Biochemistry* **2003**, *42*, 7497.

(3) Costas, M.; Mehn, M. P.; Jensen, M. P.; Que, Jr., L. *Chem. Rev.* **2004**, *104*, 939.

(4) Decker, A.; Solomon, E. I. *Angew. Chem.* **2005**, *117*, 2292.

10.1021/ic701161r CCC: $40.75
Published on Web 12/12/2007

crystal structures of nonheme Fe^{IV}═O complexes are available.[5,21,22] Various spectroscopic techniques such as electronic, MCD, Raman, and Mössbauer spectroscopy are routinely used to characterize ferryl complexes; due to mixing of the ground and the first excited-state and the resulting large zero-field splitting, EPR spectroscopy has generally been of little use.[1,4,6,23] Quantum-chemical studies (DFT as well as post Hartree−Fock calculations) have been used to understand the bonding and reactivity of heme and nonheme Fe^{IV}═O complexes.[4,6,7,23]

An important issue in Fe^{IV} coordination chemistry is the ground-state spin multiplicity. Among the three possible spin states ($S = 0$, 1, 2) the singlet state is unlikely due to the asymmetry of the formed metal complex, but both $S = 1$ and $S = 2$ ground states have been observed. The iron center in P450 has an $S = 1$ ground state,[24] that in TauD has a high-spin configuration ($S = 2$)[25] and the ferryl aqua ion also has an $S = 2$ ground state,[11] but most nonheme iron model complexes have an intermediate-spin ($S = 1$) ground state.[1,3] It has been proposed that the spin state in the nonheme iron model complexes can be tuned by the ligand sphere.[12,26,27] On the basis of a combination of experimental mechanistic and computational work, a high-spin state has been proposed for a ferryl complex with a tetradentate bispidine ligand, but so far there is no published spectroscopic evidence for any $S = 2$ nonheme Fe^{IV}═O model complex (the well-characterized aqua ion mentioned above is not considered here as a nonheme ferryl model complex).[11,28] The close-lying spin states in general complicate DFT-based mechanistic studies because various states are energetically accessible and may therefore participate in the catalytic cycle (two- or multistate reactivity). This may lead to spin-crossover, and the product distribution and yield then depend not only on the ground but also on excited states.[29]

Chart 1

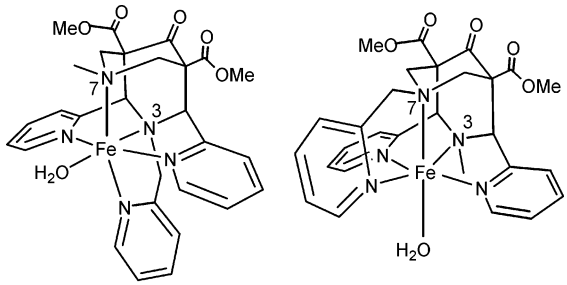

$[(L^1)Fe(OH_2)]^{2+}$ $[(L^2)Fe(OH_2)]^{2+}$

The development of synthetic iron complexes, which mimic the reactivity of nonheme iron enzymes is a competitive area of research. A number of tetra- and pentadentate nitrogen donor ligands and their Fe^{II} complexes often based on the tpa backbone [tpa = tris(2-pyridylethyl)amine] have been used in this area.[3,14,30−34] Most of these complexes are catalytically active in the oxidation of olefins in the presence of H_2O_2. In recent years, we have developed the coordination chemistry of complexes with bispidine ligands. These are very rigid and lead to an elastic coordination sphere and consequently to interesting modes of isomerism (see[35,36] for details on this seeming contradiction). A wide range of bispidine metal complexes with a variety of coordination geometries and various applications has been reported.[36] The catalytic activity of bispidine Fe^{II} complexes has been examined, and they are among the most-active iron catalysts known for the epoxidation and dihydroxylation of olefins with H_2O_2.[37] The structural versatility of the bispidine ligands offers the possibility to modify the steric and/or electronic factors and, therefore, to tune the efficiency and selectivity of the catalyst and to help to evaluate the catalytic mechanisms in detail.

The $(L)Fe^{II}/H_2O_2$ catalyst system with the isomeric pair of pentadentate bispidine ligands L^1 and L^2 has been studied in detail (Chart 1 for the ligand structures). L^1 produces more stable FeL−substrate complexes and FeL^2 is a more efficient

(5) Rohde, J.-U.; In, J.-H.; Lim, M. H.; Brennessel, W. W.; Bukowski, M. R.; Stubna, A.; Münck, E.; Nam, W.; Que, Jr., L. *Science* **2003**, *299*, 1037.
(6) Neese, F. *Biochemistry* **2006**, *100*, 716.
(7) Ghosh, A.; Tangen, E.; Ryeng, H.; Taylor, P. R. *Eur. J. Inorg. Chem.* **2004**, 4555.
(8) Kumar, D.; Hirao, H.; Que, L. J.; Shaik, S. *J. Am. Chem. Soc.* **2005**, *127*, 8026.
(9) Kamachi, T.; Kouno, T.; Nam, W.; Yoshizawa, K. *J. Inorg. Bio. Chem.* **2006**, *100*, 751.
(10) de Visser, S. P. *Angew. Chem., Int. Ed.* **2006**, *45*, 1790.
(11) Pestovsky, O.; Stoian, S.; Bominaar, E. L.; Shan, X.; Münck, E.; Que, L. J.; Bakac, A. *Angew. Chem., Int. Ed.* **2005**, *117*, 7031.
(12) Anastasi, A.; Comba, P.; McGrady, J.; Lienke, A.; Rohwer, H. *Inorg. Chem.* **2007**, *46*, 6420.
(13) Balland, V.; Charlot, M.-F.; Banse, F.; Girerd, J.-J.; Mattioli, T. A.; Bill, E.; Bartoli, J.-F.; Battioni, P.; Mansuy, D. *Eur. J. Inorg. Chem.* **2004**, 301.
(14) Shan, X.; Que, L. J. *J. Inorg. Biochem.* **2006**, *100*, 421.
(15) Dey, A.; Ghosh, A. *J. Am. Chem. Soc.* **2002**, *124*, 3206.
(16) Groves, J. T.; Gross, Z.; Stern, M. K. *J. Am. Chem. Soc.* **1994**, *33*, 5065.
(17) Berg, T. A. V.; de Boer, J. W.; Browne, W. R.; Roelfes, G.; Feringa, B. L. *J. Chem. Soc., Chem. Comm.* **2004**, 2550.
(18) Kozlowski, P. M.; Kuta, J.; Ohta, T.; Kitagawa, T. *J. Inorg. Biochem.* **2006**, *100*, 744.
(19) Terner, J.; Palaniappan, V.; Gold, A.; Weiss, R.; Fitgerald, M. M.; Sullivan, A. M.; Hosten, C. M. *Biochemistry* **2006**, *100*, 480.
(20) Grapperhaus, C. A.; Mienert, B.; Bill, E.; Weyhermüller, T.; Wieghardt, K. *Inorg. Chem.* **2000**, *39*, 5306.
(21) Decker, A.; Rohde, J. U.; Que, Jr., L.; Solomon, E. I. *J. Am. Chem. Soc.* **2004**, *126*, 5378.
(22) Klinker, E. J.; Kaizer, J.; Brennessel, W. W.; Woodrum, N. L.; Cramer, C. J.; Que, Jr., L. *Angew. Chem.* **2005**, *117*, 3756.
(23) Aquino, F.; Rodriguez, J. H. *J. Chem. Phys.* **2005**, *123*, 204902.
(24) Shaik, S.; Cohen, S.; Visser, S. P. d.; Sharma, P. K.; Kumar, D.; Kozuch, S.; Ogliaro, F.; Danovich, D. *Eur. J. Inorg. Chem.* **2004**, 207.
(25) Price, J. C.; Barr, E. W.; Glass, T. E.; Krebs, C.; Bollinger, Jr., M. *J. Am. Chem. Soc.* **2003**, *125*, 13008.
(26) Zang, Y.; Kim, J.; Dong, Y.; Wilkinson, E.; Appelman, E. H.; Que, L. J. *J. Am. Chem. Soc.* **1997**, *119*, 4197.
(27) Comba, P.; Rajaraman, G.; Rohwer, H. *Inorg. Chem.* **2007**, *46*, 3826.
(28) Bautz, J.; Comba, P.; Lopez de Laorden, C.; Menzel, M.; Rajaraman, G. *Angew. Chem., Int. Ed.* **2007**, *46*, 8067.
(29) Shaik, S.; Visser, S. P. d.; Kumar, D. *Inorg. Chem.* **2004**, *9*, 661.
(30) Balleste, R. M.; Fujita, M.; C., H.; Que, L. J. *J. Mol. Catalysis* **2006**, *251*, 49.
(31) Fujita, M.; Costas, M.; Que, L. J. *J. Am. Chem. Soc.* **2003**, *125*, 9912.
(32) Roelfes, G.; Lubben, M.; Hage, R.; Que, Jr., L.; Feringa, B. L. *Chem. Eur. J.* **2000**, *6*, 2152.
(33) Kim, S. O.; Sashi, C. V.; Seo, M. S.; Kim, J.; Nam, W. *J. Am. Chem. Soc.* **2005**, *127*, 4178.
(34) Collins, T. J. *Acc. Chem. Res.* **2002**, *35*, 782.
(35) Comba, P.; Schiek, W. *Coord. Chem. Rev.* **2003**, *238−239*, 21.
(36) Comba, P.; Kerscher, M.; Schiek, W. *Prog. Inorg. Chem.* **2007**, *55*, 613.
(37) Bukowski, M. R.; Comba, P.; Lienke, A.; Limberg, C.; Lopez de Laorden, C.; Mas-Balleste, R.; Merz, M.; Que, Jr., L. *Angew. Chem., Int. Ed.* **2006**, *45*, 3446.

Scheme 1

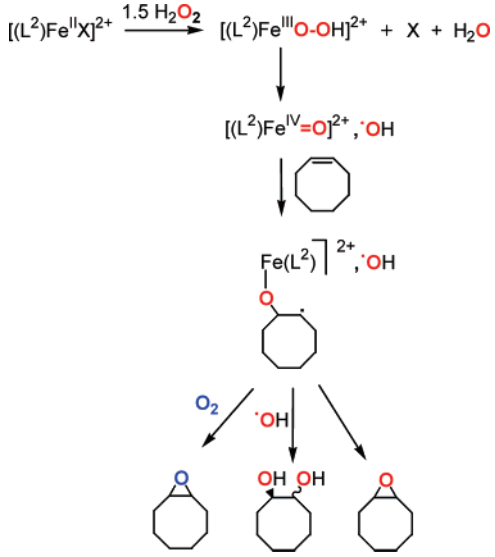

catalyst for olefin oxidation.[37,38] This has been expected from experimental structural, thermodynamic, and spectroscopic data with iron and other metal ions and is supported by computational studies.[12,27,36,39,40] Low-spin Fe^{III} hydroperoxo, high-spin Fe^{III} peroxo, and intermediate-spin ($S = 1$) Fe^{IV}═O complexes of L^1 and L^2 have been characterized spectroscopically,[38,41] and the ferryl complexes have been identified as the oxidant in the $Fe^{II}L^{1,2}/H_2O_2$/cyclooctene system.[37] In aqueous solution, the oxidation of $Fe^{II}L^{1,2}$ with H_2O_2 directly produces the Fe^{IV}═O complex.[41] This might also be the case in acetonitrile, and the observed Fe^{III} complexes might then be secondary products.[37,38] It was shown that Fe^{IV}═O alone only leads to epoxide products, that is, H_2O_2 and/or a lower-valent iron species are necessary for the diol formation.[37] The analysis of product distributions, temperature- and time-dependent studies, the comparison of experiments under aerobic and anaerobic conditions, and extensive ^{18}O labeling experiments have led to the mechanistic proposal in Scheme 1. Both catalysts with ligands L^1 and L^2 were shown to follow the same pathway, but the L^1-based catalyst reacts approximately seven times more slowly.[37] The common intermediate, proposed to accommodate all of the experimental data is a carbon-centered radical, which emerges from the asymmetric attack of the Fe^{IV}═O species at the olefin and reacts with O_2 to form epoxide in a well established autoxidation process, with caged •OH radicals (resulting from the homolysis of the Fe^{III} hydroperoxo complex) to yield cis- and trans-diol, or which cyclizes to produce epoxide (Scheme 1).[38]

Here, we use DFT calculation to explore this mechanism with the more efficient L^2-based catalyst. Some results are also reported for the catalytically less efficient L^1-based iron system and compared with the faster bispidine-based catalyst.

Computational Details

In general, multi-configuration CI calculations (especially CASSCF and CASPT2) are the methods of choice for this kind of investigation, but they are prohibitive due to the size of the systems of interest because they normally require a very large active space to obtain high-quality results.[6] DFT calculations, especially with the B3LYP hybrid functional, have been successful in predicting the energies of spin states and have been applied to understand various catalytic reactions.[42−46] There are examples where CASPT2 calculations have correctly predicted the spin ground state, whereas the B3LYP method did not.[47,48] However, it has been demonstrated that the error based on calculations with B3LYP is 10−20 kJ/mol at most.[46] Specifically, for studies of Fe^{IV}═O complexes, the B3LYP results generally agree well with results obtained from CCSD(T) calculations.[7,48,49] The success of B3LYP in predicting structures and energetics is well documented.[42−46,50−54]

Here, we have performed DFT calculations with *Jaguar 5.5*,[55] using the B3LYP functional[56−59] and the LACVP basis set, that is, a double ζ quality basis set with the Los Alamos effective core potential for iron and a 6-31G basis for the other atoms.[60,61] The optimization with this basis allows one to employ a pseudo-spectral optimization algorithm. The calculations are robust even with the large molecules studied here.[62] The B3LYP/LACVP method has been shown to give reliable results in several mechanistic studies.[63] The high-quality ligand-field-theory-based initial guess and the possibility to assign the spins on specific centers have been shown to lead to smooth convergence. Additional calculations with OPBE[64,65] and B3LYP*[66] were performed with *Gaussian 03*.[67] For comparison of the results with those based on B3LYP, the same basis set was employed. The frequency calculations on the computed transition-state structures and intermediates were done with *Jaguar* and *Gaussian 03* to confirm their nature.[55,67] The role of solvation on the energetics was studied for some of the species at the B3LYP/

(38) Bukowski, M. R.; Comba, P.; Limberg, C.; Merz, M.; Que, Jr., L.; Wistuba, T. *Angew. Chem., Int. Ed.* **2004**, *43*, 1283.
(39) Anastasi, A.; Lienke, A.; Comba, P.; Rohwer, H.; McGrady, J. E. *Eur. J. Inorg. Chem.* **2007**, *65*.
(40) Born, K.; Comba, P.; Ferrari, R.; Kuwata, S.; Lawrance, G. A.; Wadepohl, H. *Inorg. Chem.* **2007**, *46*, 458.
(41) Bautz, J.; Bukowski, M.; Kerscher, M.; Stubna, A.; Comba, P.; Lienke, A.; Münck, E.; Que Jr, L. *Angew. Chem., Int. Ed.* **2006**, *45*, 5681.
(42) Hirao, H.; Kumar, D.; Que, L. J.; Shaik, S. *J. Am. Chem. Soc.* **2006**, *128*, 8590.
(43) Hiro, H.; Kumar, D.; Thiel, W.; Shaik, S. *J. Am. Chem. Soc.* **2005**, *127*, 13007.
(44) Bathelt, C. M.; Zurek, J.; Mulholland, A. J.; Harvey, J. N. *J. Am. Chem. Soc.* **2005**, *127*, 12900.
(45) Bassan, A.; A., B. M. R.; Siegbahn, P. E. M.; Que, L. J. *Angew. Chem., Int. Ed.* **2005**, *44*, 2939.
(46) Siegbahn, P. E. M.; Borowski, T. *Acc. Chem. Res.* **2006**, *39*, 729.
(47) Gherman, B. F.; Cramer, C. J. *Inorg. Chem.* **2004**, *43*, 7281.
(48) Ghosh, A.; Taylor, P. R. *Curr. Opin. Chem. Biol.* **2003**, *7*, 113.
(49) Note that CCSD(T) is a valuable method to compare and calibrate different methodologies at the expense of very high computational time.
(50) Siegbahn, P. E. M. *J. Biol. Inorg. Chem.* **2006**, *11*, 695.
(51) Ghosh, A. *J. Biol. Inorg. Chem.* **2006**, *11*, 671.
(52) Neese, F. *J. Biol. Inorg. Chem.* **2006**, *11*, 702.
(53) Noodleman, L.; Han, W.-G. *J. Biol. Inorg. Chem.* **2006**, *11*, 674.
(54) Ghosh, A. *J. Biol. Inorg. Chem.* **2006**, *11*, 712.
(55) Schrödinger *JAGUAR 5.5*; Schrödinger, Inc.: Portland, OR.
(56) Becke, A. D. *J. Chem. Phys.* **1992**, *96*, 2155.
(57) Becke, A. D. *J. Chem. Phys.* **1992**, *97*, 9713.
(58) Becke, A. D. *J. Chem. Phys. B.* **1993**, *98*, 5648.
(59) Lee, C.; Yang, W.; Parr, R. G. *Phys. Rev. B* **1988**, *37*, 785.
(60) Hay, J. P.; Wadt, W. R. *J. Chem. Phys.* **1985**, *82*, 99.
(61) Friesner, R. A.; Murphy, R. B.; Beachy, M. D.; Ringlanda, M. N.; Pollard, W. T.; Dunietz, B. D.; Cao, Y. X. *J. Phys. Chem. A* **1999**, *103*, 1913.
(62) Hasman, D.; Beachy, M. D.; Wang, L.; Friesner, R. A. *J. Comput. Chem.* **1998**, *19*, 1017.
(63) de Visser, S. P.; Ogliaro, F.; Harris, N.; Shaik, S. *J. Am. Chem. Soc.* **2001**, *123*, 3037.
(64) Handy, N. C.; Cohen, A. J. *Mol. Phys.* **2001**, *99*, 403.

LACVP level with the polarizable continuum solvent model (PCM) with *Gaussian 03* on geometries optimized with *Jaguar* and with acetronitrile as the solvent.[68−71]

The good performance of the B3LYP hybrid functional for this kind of study is well documented.[63,72−75] However, there are some examples, where the B3LYP functional fails to predict the correct spin-state ordering in comparison with high-level CASPT2 calculations, especially for iron-containing complexes. The OPBE GGA functional, which is a combination of the optimized OPTX exchange part with the PBE correlation functional, has been described to predict the accurate spin-state ordering for iron complexes.[64,65] Although different correlation functionals have been combined with OPTX, a recent study on iron complexes indicates that PBE performs best.[76,77] Also, OPTX correlation improves the calculated energy barriers for various reactions, compared with other GGA functionals.[78] The B3LYP* hybrid functional with 15% instead of the usual 20% HF exchange was shown to predict a reasonably accurate spin-state ordering for iron complexes.[79] It has been validated for a G2 test set and first-row transition-metal complexes.[66,80] Therefore, we have also tested the performance of B3LYP* for our bispidine iron complexes.

The OPBE and B3LYP* functionals have been used to evaluate the energies of $[(L^2)Fe^{IV}{=}O]^{2+}$. In agreement with experiment and the B3LYP results, both functionals predict the $S = 1$ configuration as the ground state. The calculated energy gap between the two states with the OPBE functional is 35.7 kJ/mol, that is, approximately 4 kJ/mol smaller than with B3LYP. With B3LYP*, the difference is 46.7 kJ/mol, that is, approximately 7 kJ/mol larger than with B3LYP. The B3LYP standard method performs well for iron complexes in higher oxidation states and also predicts the correct spin state for Fe^{III}.[81,82] A wrong prediction of the spin-state ordering with the OPBE functional for nonheme $Fe^{IV}{=}O$ complexes was also reported.[42] Extensive literature data show that the calculated spin-state splitting in transition-metal complexes in general strongly depends on the amount of exact exchange.[83] For complexes with ligands such as halides, water, ammonia, and other nitrogen-based ligands, the functional with 20% exact exchange provides accurate results,[83] and our bispidine complexes fall into this category. For all of these reasons, we have used the standard B3LYP functional for the majority of the calculations, and only a few computations were performed with the OPBE and B3LYP* functionals.

The expected error limit of B3LYP calculations is in the range of 10−20 kJ/mol.[46] The energetics of the majority of species and spin states reported here are within 50 kJ/mol and, therefore, an error of 20 kJ/mol is significant. High-level ab initio calculations would be required to obtain a more accurate estimate of the error limits for our systems. However, the qualitative conclusions reported here are valuable, especially in comparison with the published experimental data.[37]

Results

On the basis of the experimental observations given in Scheme 1, the four reaction channels (path 1 to path 4) of Scheme 2 were studied with DFT calculations. For the epoxidation, $Fe^{IV}{=}O$ can react with cyclooctene either in a concerted (path 1) or in a consecutive reaction (path 2). The concerted mechanism directly yields the epoxide product through *tsI*, with the ferryl oxygen atom inserted in the C=C bond. In the stepwise reaction, the $Fe^{IV}{=}O$ oxidant attacks the olefin asymmetrically in *tsII* to yield the Fe^{III} radical intermediate *intII*. This undergoes cyclization through *tsIII* to produce the epoxide. The radical intermediate *intII* may also react with molecular O_2 (path 3) to yield the alkylperoxy radical species *intIII* through *tsIV*, and this produces epoxide with the oxygen atom arising from molecular O_2. Path 4 leads to the formation of diol products through *tsV*, where the $^{\bullet}$OH radical reacts with *intII* to produce *intIV*. It is important to note that free $^{\bullet}$OH radicals, derived from the homolytic cleavage of the Fe^{III} hydroperoxo complex, are unlikely to be directly involved in the olefin oxidation reaction, as these are extremely reactive and, therefore, very short-lived in nonaqueous solution.[84,85] Note that the mechanism derived from experiment [reactions based on Fe^{II}/H_2O_2 solutions and on in situ-prepared $Fe^{IV}{=}O$; product analyses (epoxide, cis and trans diols) and extensive ^{18}O labeling studies ($H_2{}^{18}O_2$, $H_2{}^{18}O$, $^{18}O_2$)] has, as a basic element, *intII* as the common intermediate (Scheme 1).[37] That is, path 2 and path 3 are proposed to produce the epoxide and path 4 to lead to the cis and trans diol products. The concerted path 1 was

(65) Perdew, J. P.; Burke, K.; Ernzerhof, M. *Phys. Rev. Lett.* **1996**, *77*, 3865.
(66) Salomon, O.; Reiher, M.; Hess, B. A. *J. Chem. Phys.* **2002**, *117*, 4729.
(67) Frisch, M. J.; Trucks, G. W.; Schlegel, H. B.; Scuseria, G. E.; Robb, M. A.; Cheeseman, J. R.; Montgomery, J. A., Jr.; Vreven, T.; Kudin, K. N.; Burant, J. C.; Millam, J. M.; Iyengar, S. S.; Tomasi, J.; Barone, V.; Mennucci, B.; Cossi, M.; Scalmani, G.; Rega, N.; Petersson, G. A.; Nakatsuji, H.; Hada, M.; Ehara, M.; Toyota, K.; Fukuda, R.; Hasegawa, J.; Ishida, M.; Nakajima, T.; Honda, Y.; Kitao, O.; Nakai, H.; Klene, M.; Li, X.; Knox, J. E.; Hratchian, H. P.; Cross, J. B.; Bakken, V.; Adamo, C.; Jaramillo, J.; Gomperts, R.; Stratmann, R. E.; Yazyev, O.; Austin, A. J.; Cammi, R.; Pomelli, C.; Ochterski, J. W.; Ayala, P. Y.; Morokuma, K.; Voth, G. A.; Salvador, P.; Dannenberg, J. J.; Zakrzewski, V. G.; Dapprich, S.; Daniels, A. D.; Strain, M. C.; Farkas, O.; Malick, D. K.; Rabuck, A. D.; Raghavachari, K.; Foresman, J. B.; Ortiz, J. V.; Cui, Q.; Baboul, A. G.; Clifford, S.; Cioslowski, J.; Stefanov, B. B.; Liu, G.; Liashenko, A.; Piskorz, P.; Komaromi, I.; Martin, R. L.; Fox, D. J.; Keith, T.; Al-Laham, M. A.; Peng, C. Y.; Nanayakkara, A.; Challacombe, M.; Gill, P. M. W.; Johnson, B.; Chen, W.; Wong, M. W.; Gonzalez, C.; Pople, J. A. *Gaussian 03*, revision B.03; Gaussian, Inc.: Wallingford, CT, 2004.
(68) Cancès, M. T.; Mennucci, B.; Tomasi, J. *J. Chem. Phys.* **1997**, *107*, 3032.
(69) Cossi, M.; Barone, B.; Mennucci, B.; Tomasi, J. *Chem. Phys. Lett.* **1998**, *286*, 253.
(70) Mennucci, B.; Tomasi, J. *J. Chem. Phys.* **1997**, *106*, 5151.
(71) Cossi, M.; Scalmani, G.; Raga, N.; Barone, V. *J. Chem. Phys.* **2002**, *117*, 43.
(72) Bassan, A.; Blomberg, M. R. A.; Siegbahn, P. E. M. *Chem.—Eur. J.* **2003**, *9*, 4055.
(73) Bassan, A.; Blomberg, M. R. A.; Siegbahn, P. E. M. *J. Biol. Inorg. Chem.* **2004**, *9*, 439.
(74) Bassan, A.; Blomberg, M. R. A.; Siegbahn, P. E. M.; Que Jr. L. *Chem.—Eur. J.* **2005**, *11*, 692.
(75) Quinonero, D.; Morokuma, K.; Musaev, D. G.; Morokuma, K.; Mas-Balleste, R.; Que, J., L. *J. Am. Chem. Soc.* **2005**, *127*, 6548.
(76) Swart, M.; Groenhof, A. R.; Ehlers, A. W.; Lammertsma, K. *J. Phys. Chem. A* **2004**, *108*, 5479.
(77) Swart, M.; Whilers, A. W.; Lammertsma, K. *Mol. Phys.* **2004**, *102*, 2467.
(78) Gruning, M.; Grisenko, O. V.; Baerends, E. J. *J. Phys. Chem. A* **2004**, *108*, 4459.
(79) Reiher, M.; Salomon, O.; Hess, B. A. *Theor. Chem. Acc.* **2001**, *107*, 48.
(80) Reiher, M. *Inorg. Chem.* **2002**, *41*, 6928.
(81) Chang, C. H.; Boone, A. J.; Bartlett, R. J.; Richards, N. G. *J. Inorg. Chem.* **2004**, *43*, 458.
(82) Fallon, G. D.; Gatehouse, B. M.; Minari, P. J.; Murray, K. S.; West, B. O. *J. Chem. Soc., Dalton Trans.* **1984**, 2733.
(83) Harvey, J. N. *Annu. Rep. Prog. Chem., Sect. C.* **2006**, *102*, 203.
(84) Neta, P.; Schuler, R. H. *J. Phys. Chem.* **1975**, *79*, 1.
(85) Buxton, G. V.; Greenstock, C. L.; Helman, W. P.; Ross, A. B. *J. Phys. Chem.* **1988**, 513.

Scheme 2

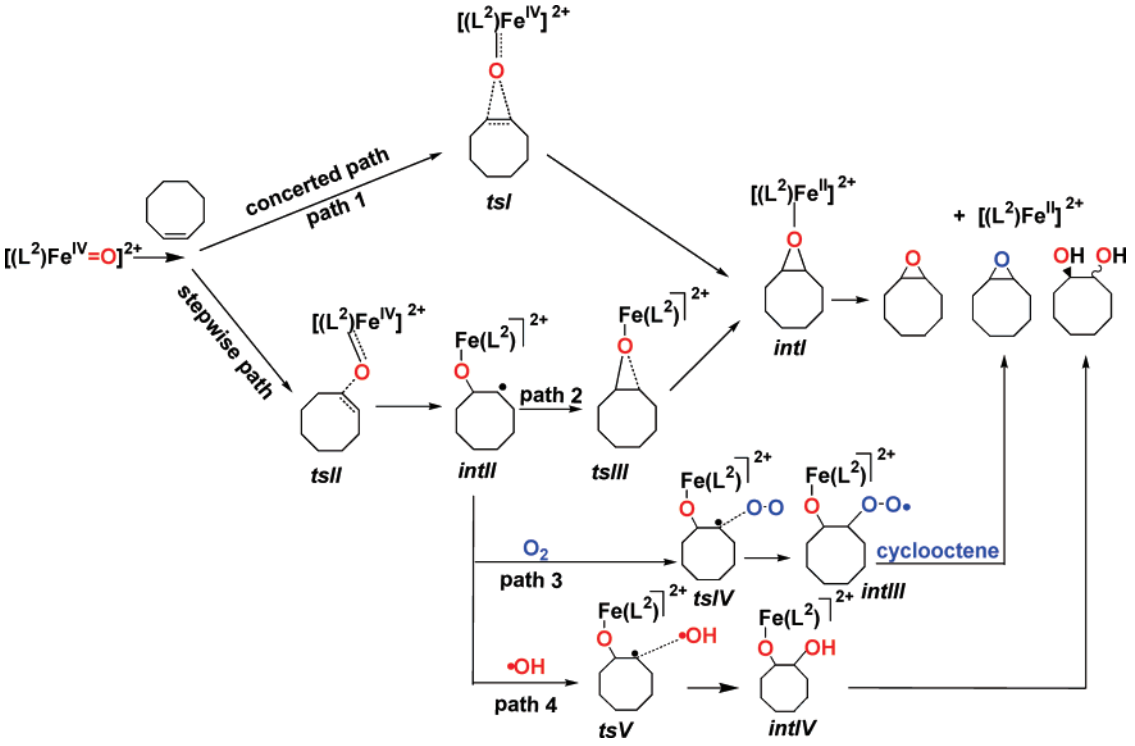

neglected for simplicity in the experimental study, although, on the basis of the combined experimental data, it cannot be excluded as a minor, alternative parallel reaction channel, and it therefore was included in the DFT analysis. Fe^{IV}═O ($S = 1$) has been shown to be a relevant product in $Fe^{II}L^{1,2}/H_2O_2$ systems (experiments without alkene substrates) and that in situ-prepared $(L^{1,2})Fe^{IV}$═O transfers its ferryl oxygen atom to the cyclooctene double bond.[37,41] From published work on the •OH radical-induced oxidation of cyclooctene, it is known that autoxidation primarily leads to epoxide, and the mechanism derived from the thorough experimental study is similar to that proposed in Scheme 2, path 3.[86] The importance of the radical intermediate *intII* is derived from the fact that there is *cis*- as well as *trans*-1,2-diol product, and that this disappears in MeOH as a solvent, which is known to efficiently quench •OH radicals.[37] The oxygen atoms that arise from $H_2{}^{18}O$ have been proposed to result from water-exchange with the ferryl oxygen atom.[37]

Before we discuss in detail structures and energetics of the intermediates and transition states from Scheme 2, it is necessary to assess the validity of the computational methods used to obtain information on the electronics of the Fe^{III} and Fe^{IV} complexes. The next section therefore discusses the electronic structure of the ferryl complexes.[87]

The Electronic Structure of the $[(L^{1,2})Fe^{IV}$═O$]^{2+}$ Complexes. Spectroscopic studies of $[(L^{1,2})Fe^{IV}$═O$]^{2+}$ reveal that these compounds have an $S = 1$ spin ground state.[41] For the L^2 complex, DFT calculations have been performed on the $S = 1$ (*is*) and $S = 2$ (*hs*) spin states. The results are consistent with the experimentally observed $S = 1$ ground state.[88] The $S = 2$ state is 40 kJ/mol (PCM, 44 kJ/mol) above the triplet ground state. The optimized structure and the singly occupied MOs of the $S = 1$ state are shown in Figure 1; selected computed bond distances and angles for the different spin states are given in Table 1. The Fe−O bond is short (1.65 Å), as expected from experimental data of other ferryl complexes,[5,21,22] and the Fe−N7 bond is elongated (2.21 Å); the bond to the other tertiary amine (Fe−N3) is considerably shorter (2.02 Å). The d_{xy} orbital is doubly, d_{xz} and d_{yz} are singly occupied. The SOMOs are almost degenerate and have large contributions from oxygen. This is seen in the spin distribution, where the unpaired electrons of the Fe^{IV} center are delocalized to the ferryl oxygen (Table 2). The oxygen-centered orbitals are antibonding combinations with the metal d orbitals. The unoccupied $d_{x^2-y^2}$ and d_{z^2} orbitals are antibonding, and the antibonding character of the d_{z^2} orbital is along N7−Fe−O. The *hs* state has the electronic configuration $(d_{xy})^1(d_{xz})^1(d_{yz})^1(d_{x^2-y^2})^1(d_{z^2})^0$. All of the Fe−N bonds are longer in the *hs* than in the *is* state, with the exception of Fe−N7 and Fe−O along the *z* direction, which are slightly shorter (Fe−O = 1.646 vs 1.651 Å and Fe−N7 = 2.183 vs 2.210 Å). This is consistent with the electronic configuration given above and the result of a subtle combination of various electronic effects (trans influence and Jahn−Teller-type effects), which also influence the relative stabilities of the spin states.[12] Both the *is* and the *hs* states are energetically accessible and, therefore, the possibility of two-state reactivity arises.

(86) van Sickle, D. E.; Mayo, F. R.; Arluck, R. M. *J. Am. Chem. Soc.* **1965**, *87*, 4824.

(87) A more rigorous analysis is published elsewhere. That investigation is based on a slightly different computational model and basis set but arrives at similar conclusions with respect to the relative spin-state stabilities. [12]

(88) See supporting information for a discussion of the $S = 0$ state.

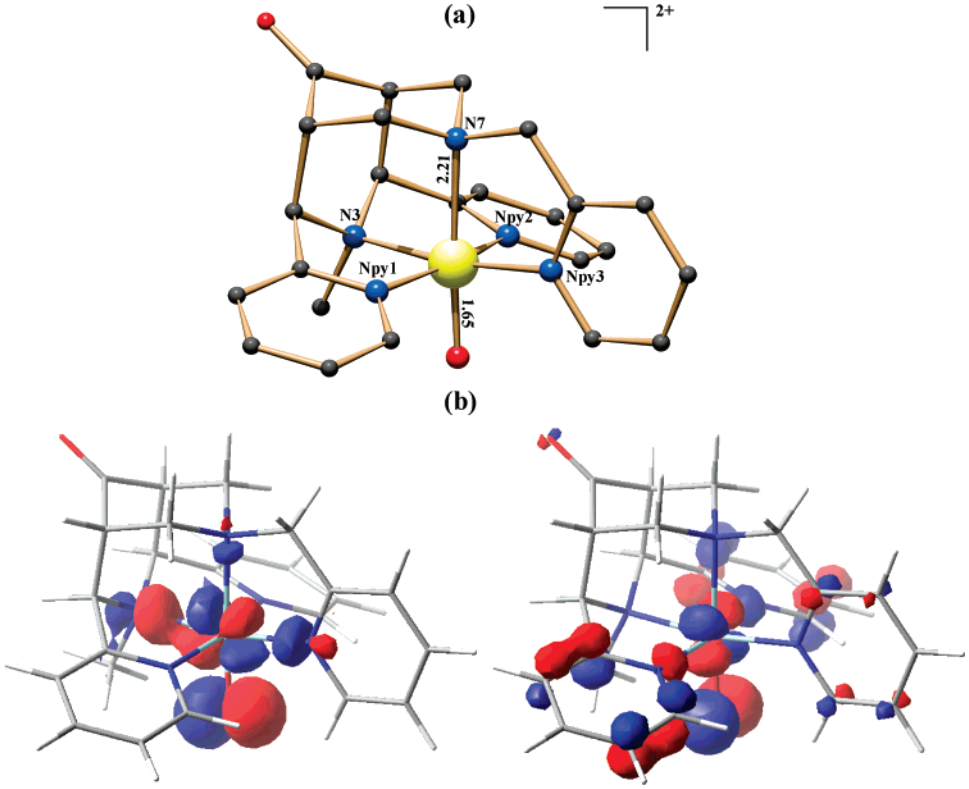

Figure 1. (a) B3LYP-optimized structure of $[(L^2)Fe^{IV}{=}O]^{2+}$ in the $S = 1$ state. (b) Plots of the magnetic orbitals of the $S = 1$ state; all of the bond lengths are given in angstroms and angles are given in degrees.

For the L^1 complex, the $S = 2$ state is 44 kJ/mol higher in energy than the $S = 1$ ground state. The optimized structures are listed in Table 1 (Figure SF4 of the Supporting Information for plots of the optimized structures and the MOs of the $S = 1$ state). The L^1 complex is 11.6 kJ/mol more stable than the isomeric L^2 complex. The structural parameters and spin densities (Tables 1 and 2) of the L^1 and L^2 ferryl complexes in the $S = 1$ state are very similar. Therefore, the energy difference is assumed to be due to the ligand-induced strain. These effects are known in bispidine complexes and have been studied in detail for the corresponding Cu^{II} complexes.[89−92]

Epoxidation: The Ferryl Oxygen Transfer and the O_2 Reaction Paths. The Concerted and the Stepwise Mechanism (Path 1 and Path 2). The search for a concerted transition state required a relaxed potential-energy scan, where the distance between the ferryl oxygen and the two olefinic carbon atoms was varied prior to the refinement of the transition state. The resulting energy barrier is in the expected range (46 kJ/mol), but the corresponding structure is a second-order saddle point, and, therefore, this path is not included in the mechanistic discussion.[93] In the stepwise reaction, the olefin approaches the $Fe^{IV}{=}O$ center in an end-on fashion (*tsII*). The formation of the O−C bond leads to the Fe^{III}−radical intermediate *intII*. This may undergo cyclization to lead to the Fe^{II}−epoxide product *intI*. The calculated energy barrier for *tsII* is 36 kJ/mol, the optimized structure is shown in Figure 2, and the structural data are given in Table 1. The Fe−O as well as the C=C bonds are elongated with respect to the reactant. The spin densities on the iron and oxygen atoms are partially delocalized to the adjacent olefinic carbon atom (Table 2). The calculated barrier with solvation included is 86 kJ/mol. The large increase in the barrier height, compared to the gas phase, is probably due to the stronger solvation of the dicationic $[(L^2)Fe^{IV}{=}O]^{2+}$ complex, compared to the corresponding transition state *tsII* species, where the charge is diffused over the catalyst−cyclooctene complex. We have computed solvation for the entire reaction profile of the L^2-based system but have limited our discussion to the gas-phase energetics, as these have also been found in other studies to generally be in better agreement with the experimental results, particularly for nonheme $Fe^{IV}{=}O$ complexes.[42]

In *intII*, five 3d electrons are located on iron and one on the substrate carbon radical. The spin on the Fe^{III} center can be *hs* ($^5/_2$), *is* ($^3/_2$), or *ls* ($^1/_2$), and there are three possible total spin states $S_T = 1$, 2, or 3 with ferromagnetic coupling between the iron and the carbon radical centers, and another three with antiferromagnetic coupling ($S_T = 0$, 1, 2). The exchange interaction between the iron center and the carbon radical leads to a very small splitting between the ferromagnetic and antiferromagnetic states on the order of a few hundred wave numbers. For example, for *hs* Fe^{III}, there are

(89) Atanasov, M.; Comba, P.; Martin, B.; Müller, V.; Rajaraman, G.; Rohwer, H.; Wunderlich, S. *J. Comput. Chem.* **2006**, *27*, 1263.
(90) Atanasov, M.; Comba, P. Work in progress.
(91) Comba, P.; Lienke, A. *Inorg. Chem.* **2001**, *40*, 5206.
(92) Bleiholder, C.; Börzel, H.; Comba, P.; Ferrari, R.; Heydt, A.; Kerscher, M.; Kuwata, S.; Laurenczy, G.; Lawrance, G. A.; Lienke, A.; Martin, B.; Merz, M.; Nuber, B.; Pritzkow, H. *Inorg. Chem.* **2005**, *44*, 8145.
(93) See supporting material for the potential-energy scan and the computed structure of *tsI*.

Table 1. Selected Geometric Parameters of the Optimized (B3LYP/LACVP) Structures of the Iron Complexes in the Catalytic Oxidation Reaction of Cyclooctene with H_2O_2 with the L^1- and L^2-Based Iron Complexes[a,b]

	Interatomic distances (Å) and angles (°)										
	Fe−O	Fe−N7	Fe−N3	Fe−N_{py1}	Fe−N_{py2}	Fe−N_{py3}	O−C_a	O−C_b	C_a−C_b	Fe−O−C_a	O−C_a−C_b
$[L^2Fe^{IV}{=}O]^{2+}$											
$S = 0$	1.68	2.20	2.01	2.01	2.01	1.99					
$S = 1$	1.65	2.21	2.02	2.01	2.01	1.98					
$S = 2$	1.65	2.18	2.08	2.17	2.17	2.04					
tsI											
$S = 1$	1.86	2.46	2.05	2.00	2.01	2.04	2.04	2.05	1.41		
$S = 2$	1.73	2.41	2.23	2.15	2.19	2.13	2.22	2.40	1.39	177.5	79.9
tsII											
$S = 1$	1.78	2.27	2.04	2.02	2.01	2.01	2.00		1.41	137.5	99.9
intII											
$S_T = 3$	1.80	2.43	2.23	2.17	2.32	2.15	1.48		1.50	175.0	109.2
$S_T = 1$[c]	1.82	2.21	2.24	2.14	2.21	2.15	1.48		1.50	134.3	107.6
$S_T = 1$	1.81	2.21	2.04	2.08	2.21	2.01	1.47		1.51	132.9	110.7
tsIII											
$S_T = 3$	2.02	2.38	2.22	2.08	2.07	2.15	1.52	1.79	1.49	146.3	72.9
$S_T = 1$[c]	1.82	2.21	2.04	2.02	2.01	2.01	1.51	2.38	1.50	132.4	106.4
$S_T = 1$	1.82	2.19	2.24	2.14	2.21	2.14	1.50	2.45	1.51	134.1	110.8
intI											
$S = 2$	2.21	2.39	2.23	2.19	2.39	2.16	1.54	1.54	1.49	145.8	61.1
$S = 1$	2.30	2.43	2.06	1.99	2.43	2.02	1.54	1.54	1.49	143.8	61.1
$S = 0$	2.17	2.14	2.05	2.00	2.14	2.03	1.53	1.53	1.49	137.9	60.9
tsIV											
$S_T = 4$[d]	1.83	2.49	2.25	2.16	2.22	2.15	1.46		1.52	157.0	
intIII											
$S = 3$	1.82	2.48	2.23	2.14	2.20	2.15	1.45		1.54	162.0	
$[L^1Fe^{IV}{=}O]^{2+}$											
$S = 1$	1.65	2.15	2.06	1.99	1.99	1.98					
$S = 2$	1.65	2.25	2.08	2.11	2.11	2.10					
tsII											
$S = 1$	1.79	2.20	2.08	2.01	2.01	2.01	1.90		1.41	152.8	108.1
intII											
$S_T = 3$	1.81	2.34	2.27	2.18	2.20	2.15	1.47		1.51	157.9	112.6
intI											
$S = 2$	2.14	2.37	2.24	2.21	2.24	2.20	1.51	1.56	1.34	144.2	62.0
$[L^2Fe^{III}OOH]^{2+}$											
$S = {}^1/_2$	1.81	2.14	2.02	2.01	2.02	1.99	1.51			117.1	
$S = {}^3/_2$	1.81	2.14	2.21	2.13	2.17	2.09	1.50			116.7	
$S = {}^5/_2$	1.92	2.33	2.21	2.15	2.18	2.12	1.47			121.5	
tsVI											
$S = 1$	1.79	2.18	2.02	1.99	2.01	1.99	1.63	2.52	1.54	176.6	98.8
tsVII											
$S = {}^1/_2$	1.74	2.21	2.02	2.03	1.99	1.99	1.94	2.10	1.38	122.7	89.9

[a] The Fe-Npy3 bond in L^1 is the Fe−pyridine distance trans to N3, and in L^2 it is trans to N7. [b] See Figure 3 for the labels C_a and C_b. [c] Antiferromagnetic $S = 1$ state for the *is* configuration on iron and spin down on the radical center. [d] In *tsIV* and *intIII*, the C_b−O distances are 1.84 and 1.54 Å, the O−O distances are 1.54 and 1.38 Å, and the C_b−O−O angles are 179.1 and 112.6 Å, respectively.

two possible spin states, one with spin up on the carbon radical (ferromagnetic interaction, total spin ground state of $S_T = 3$) and the other with spin down on the carbon radical (antiferromagnetic interaction, total spin ground state of $S_T = 2$). The geometry optimization was carried out for the ferromagnetically coupled systems with three different spin configurations on iron.[94] The broken symmetry formalism needs to be used to calculate the energy of the antiferromagnetic states. This provides a reliable estimate for the exchange interaction but often leads to SCF convergence problems, and sometimes spin projection is mandatory. The high-spin states are single determinant wavefunctions and can be treated within the DFT formalism. Therefore, wherever possible the high-spin states were studied. Convergence to correct spin states was achieved with the *hs* ($S_T = 3$) and the *ls* ($S_T = 1$) configurations on iron but not for the *is* spin state (spin density distributions in Table 2). Convergence of the *is* spin configuration on iron was obtained for the antiferromagnetic state $S_T = 1$ (spin down on the carbon-based radical).

The optimized structure of the $S_T = 3$ state of *intII* is shown in Figure 2. The main difference in structural parameters between the three spin states is the Fe−O−C angle, which varies between 175.0 and 132.9 degrees, depending on the spin configuration of the iron center. The Fe−O bond lengths are longer than in the $Fe^{IV}{=}O$ complex and the *tsII* transition state (Table 1). The Fe−N7 bond length gradually increases from $Fe^{IV}{=}O$ to *tsII* to *intII* ($S_T = 3$) from 2.21 to 2.43 Å. The $S_T = 3$ state of *intII* is the lowest in energy, and the reaction to the radical intermediate ($S_T = 3$) is thermodynamically favorable with a reaction energy of −30 kJ/mol (PCM, +25 kJ/mol). The structures with *ls*

(94) It is known that the structural differences between the spin states due to exchange interaction are negligible (ref 95 and references therein).

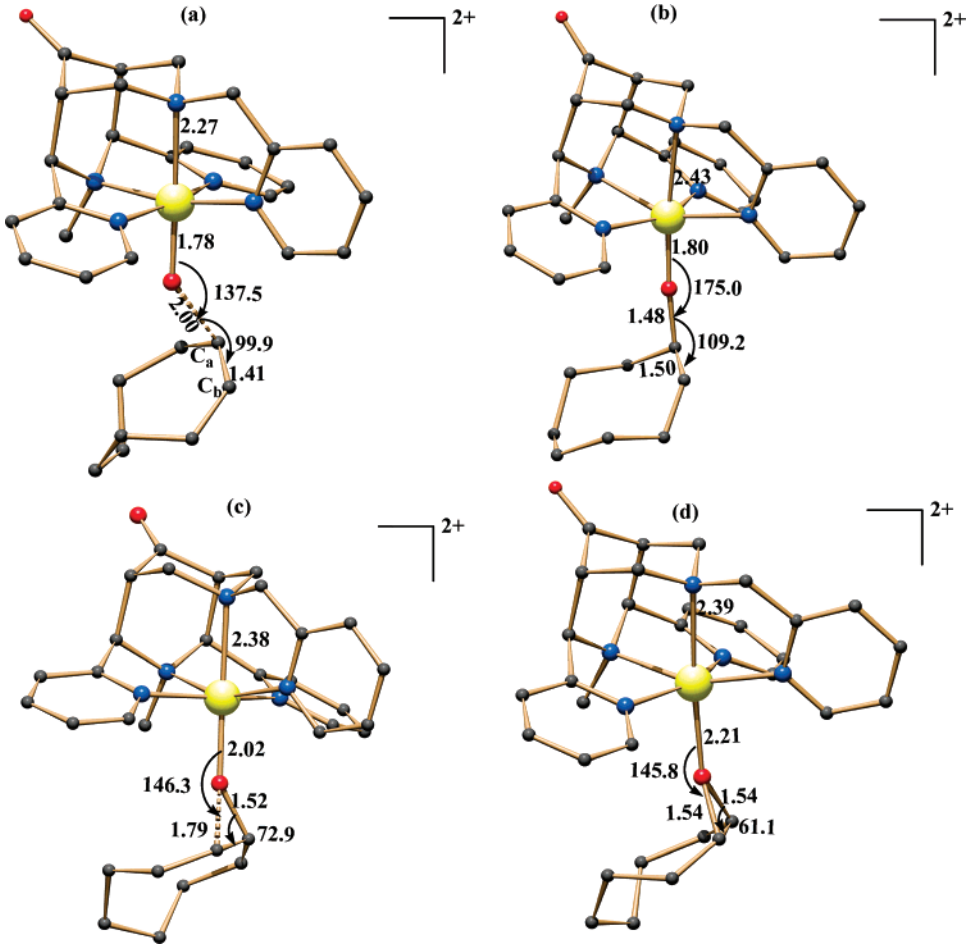

Figure 2. B3LYP-optimized structures of (a) *tsII* in the $S = 1$ configuration, (b) *intII* in the $S_T = 3$ configuration, (c) *tsIII* in the $S_T = 3$ configuration, (d) *intI* in the $S = 2$ configuration. All of the bond lengths are given in angstroms and the angles are given in degrees.

Table 2. Spin Densities of Various Species on the Potential-Energy Surface (B3LYP)[a]

spin density		Fe	O	C_a	C_b
L^2Fe^{IV}=O	$S = 1$	1.073	0.993		
	$S = 2$	2.958	0.766		
	$S = 0$	0.000	0.000		
tsI	$S = 1$	1.719	0.146	0.220	−0.027
tsII	$S = 1$	0.826	0.712	−0.104	0.630
intII	$S = 3$	3.950	0.557	−0.068	1.046
	$S = 1$	0.822	0.248	−0.097	1.011
	$S = 1$[b]	2.867	−0.029	0.089	−1.00
tsIII	$S = 3$	4.100	0.125	0.001	0.185
	$S = 1$	0.821	0.229	−0.097	1.010
	$S = 1$[b]	2.720	0.047	0.069	−0.935
intI	$S = 2$	3.750	0.017	0.007	0.010
	$S = 1$	1.996	0.011	0.008	0.012
	$S = 0$	0.000	0.000	0.000	0.000
WC		2.810	0.838	0.001	0.001
tsII		3.328	0.316	0.017	0.038
L^1Fe^{IV}=O	$S = 1$	1.092	0.966		
	$S = 2$	2.958	0.751		
tsII	$S = 1$				
intII	$S = 3$	3.968	0.508	−0.790	1.049
intI	$S = 2$	3.756	0.019	0.012	0.012

[a] See Figure 3 for the labels C_a. [b] Antiferromagnetic $S = 1$ state for the *is* configuration on iron and spin down on the radical center.

and *is* configurations on the iron center are 12.5 and 44.4 kJ/mol higher in energy, respectively. To calculate the exchange interaction between the metal center and the radical atom, the energy of both ferromagnetic and antiferromagnetic states are required. Therefore, a single point calculation was done on the $S_T = 3$ structure (spin down on the radical ion), and this yields a splitting of the state of -402.5 cm^{-1} due to exchange, and the antiferromagnetic state is the ground state (with the method used in ref 95 the calculated J value is -134.2 cm^{-1}, using the $H = -JS_1S_2$ formalism; Supporting Information for details).

The spin density plot of the $S_T = 3$ state and some key orbitals (the radical orbital and the d_{z^2} and $d_{x^2-y^2}$ type orbitals) are shown in Figure 3. The spin density on the iron center has a spherical shape, and the spin is delocalized to the coordinated atoms by spin delocalization and spin polarization. The spin density on the carbon atom has a p-orbital-type shape and is delocalized to the other carbon atoms of cyclooctene by spin polarization.

The structures of *tsII* and *intII* have also been optimized with OPBE and B3LYP*. The corresponding energy barriers are 103 and 63 kJ/mol for the OPBE and B3LYP* functionals, respectively. Both OPBE and B3LYP* overestimate the energy barrier with respect to B3LYP. Especially for *intII*, the results are significantly different with the three functionals. OPBE and B3LYP* predict the energy of *intII* higher than that of the reactant, with a reaction energy of +41 and

(95) Ruiz, E.; Alvarez, S.; Rodriguez-Fortea, A.; Alemany, P.; Pouillon, Y.; Massobrio, C. *Magnetism: Molecules to Materials II*; 2001; Vol. II.

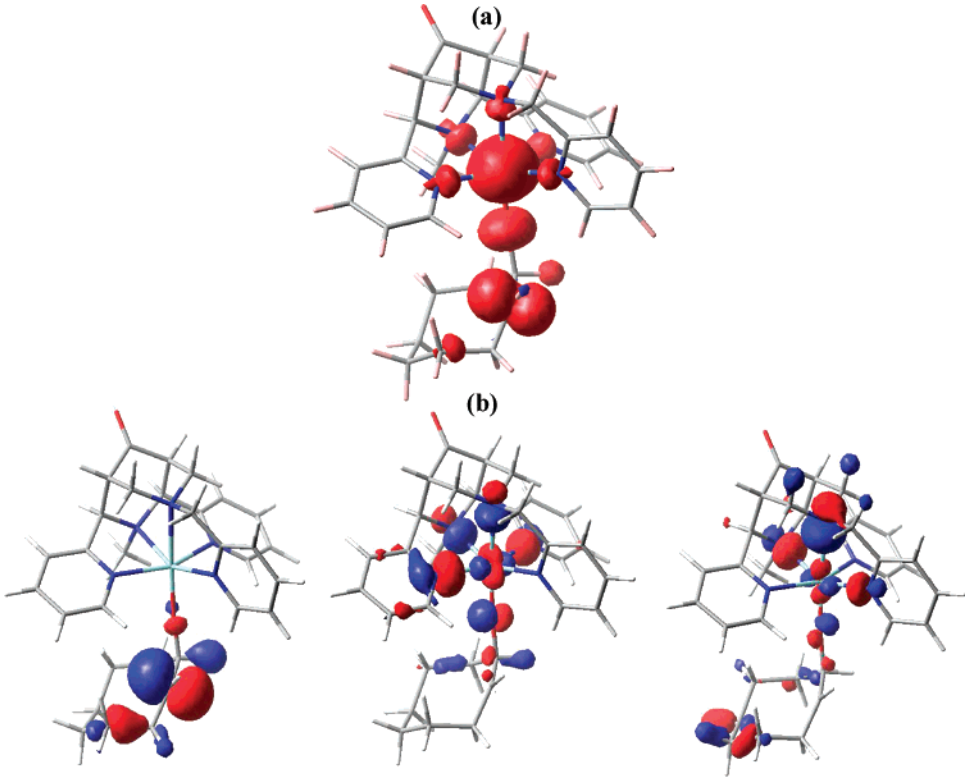

Figure 3. (a) Spin density plot of *intII* in the $S_T = 3$ configuration, (b) the key orbital of the $S_T = 3$ configuration (radical orbitals, the d_{z^2} and $d_{x^2-y^2}$ orbitals of the iron center).

Table 3. Calculated Spin Densities of Fe^{IV}=O, *tsII*, and *intII* as a Function of the Functional[a]

		OPTX-PBE	B15LYP	B3LYP
L^2Fe^{IV}=O				
$S = 1$	Fe	1.198	1.155	1.073
	O	0.931	0.943	0.993
$S = 2$	Fe	2.967	2.901	2.958
	O	0.771	0.794	0.766
tsII				
$S = 1$	Fe	1.090		0.826
	O	0.519		0.712
	C_a	−0.080		−0.104
	C_b	0.592		0.630
intII				
$S_T = 3$	Fe	3.897	3.946	3.950
	O	0.580	0.587	0.557
	C_a	−0.067	−0.020	−0.068
	C_b	1.073	0.939	1.046

[a] See Figure 3 for the labels C_a and C_b.

+71 kJ, respectively.[96] These discrepancies, especially with respect to the energy of *intII*, may be due to the fact that B3LYP overestimates the stability of high-spin states.[79,83] The computed spin densities with various functionals are given in Table 3. A more thorough interpretation would require experimental data, which are not available for this species.

The next reaction step in path 2 is the cyclization to *intI*. On the $S_T = 3$ surface, the calculated barrier is 196 kJ/mol (PCM, 241 kJ/mol). The optimized structure of *tsIII* is shown in Figure 2. The search for the transition state with *hs* configuration on iron and spin down on the radical center collapsed to *intII*. The calculated energy barriers for the *ls* and *is* iron configurations ($S_T = 1$ as in *intII*) are 12 and 21 kJ/mol, respectively.[97] The newly forming O−C interaction in the transition state is relatively short on the $S_T = 3$ surface (1.79 vs 2.38 or 2.45 Å, Table 1 and Figure 2). This is probably due to the fact that there are no empty d orbitals on the iron center to accommodate the electron from the carbon radical and is one of the reasons for the very high-energy barrier. Therefore, in this step a spin-crossover is expected before the formation of the epoxide product. The calculated spin densities of the transition states are collected in Table 2. For the $S_T = 3$ transition state *tsIII*, the spin density on the carbon radical is dramatically reduced compared to that of the $S_T = 1$ structure. The relative energies of the various spin states of *intII*, *tsIII*, and *intI* also suggest that spin changes may be involved during the cyclization reaction. Therefore, we have computed the minimum energy crossing point (MECP) for the spin crossover between the $S_T = 3$ and $S_T = 1$ surfaces with a well-established procedure, adapted to DFT calculations.[44,83,98] These calculations, performed with the *Gaussian 03* suite of programs, are computationally very expensive. Therefore, we have limited our study to the most important crossing point on the potential-energy surface, that is, the $S_T = 3$ and $S_T = 1$ surfaces of the *intII* to *intI* conversion. The optimized structure and energies of the spin states during the optimization are given

(96) Note that only the $S = 2$ state for *intII* has been calculated. The OPBE and B3LYP* methods might predict a different ordering of the spin states than B3LYP, but this possibility has not been verified.

(97) The computed barrier height with solvation included on the ls surface is 70 kJ/mol; this energy barrier did not converge in the PCM G03 calculations.

(98) Harvey, J. N.; Aschi, M.; Schwarz, H.; Koch, W. *Theor. Chem. Acc.* **1998**, *99*, 95.

Scheme 3

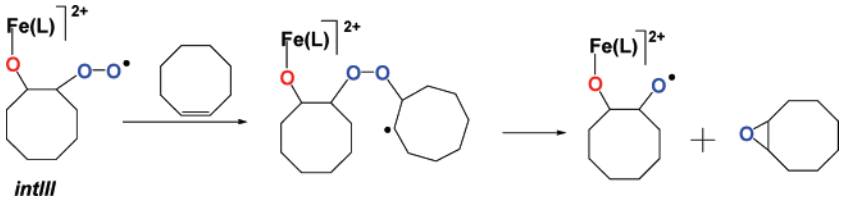

in the Supporting Information (Figures SF8 and SF9). The geometry of the MECP is similar to that of *intII* on the $S_T = 3$ surface, but the Fe−O−C angle is significantly smaller than that of *intII* in the $S_T = 3$ state and is larger than that of *intII* in the $S_T = 1$ state (168 vs 175°).

Cyclization leads to the formation of an Fe^{II}−epoxide complex, which then cleaves to produce the epoxide and the catalyst precursor. The Fe^{II}−epoxide product has been optimized with *hs* ($S = 2$), *is* ($S = 1$), and *ls* ($S = 0$) configuration on the iron center, and the $S = 2$ state is found to be the ground state. This step is exothermic, with a total reaction energy of −155 kJ/mol (PCM, −83 kJ/mol). The $S = 1$ and $S = 0$ states are 50.6 and 39.0 kJ/mol (PCM, −45 and −61 kJ/mol) higher in energy than the $S = 2$ state, respectively. The optimized structure of the $S = 2$ state is shown in Figure 2. The metal−ligand bond lengths of the $S = 2$ structure are slightly longer than those of the $S = 1$ and $S = 0$ states, except for the Fe−O and Fe−N7 bond of the $S = 1$ structure, which undergo a Jahn−Teller type elongation (Table 1). For the $S = 2$ and $S = 1$ states, the electron density is essentially localized on iron (Table 2).

The Reaction with O_2 (path 3). In this path, molecular oxygen from air reacts with the radical intermediate *intII* to form the alkylperoxy radical intermediate *intIII* via transition state *tsIV* (Scheme 2). On the basis of extensive mechanistic work on the •OH radical-induced process, *intIII* is expected to undergo autoxidation, and a possible mechanism is shown in Scheme 3.[37,86] As a result of the complexity of the species involved and various other possible scenarios, no further calculations were performed to study these steps in more detail. For the same reasons, the reaction was only studied with the $S_T = 3$ state of *intII* and with a triplet state of O_2. The pathway considered here is straight forward, and this is only the first step in the autoxidation process. Experimental support for this mechanism comes from published work. Species along this reaction path have been trapped and spectroscopically characterized. It has been shown that the reaction with O_2 (the formation of peroxy radical compounds) enhances the stability of the radical intermediate, and this is essential for the autoxidation process in our reaction.[99] A normal transition-state search to locate *tsIV* was unsuccessful. Therefore, a tight potential-energy surface scan was performed to locate the maximum along the C−O_2 coordinate. The result with a maximum energy point at 1.8 Å is shown in Figure 4. The corresponding structure was used for the transition-state optimization, and this yielded *tsIV* with an energy barrier of 99 kJ/mol (PCM, 101 kJ/mol). The optimized structures of *tsIV* and *intIII* are plotted in Figure 5, and structural data are given in Table 1. Major differences between the two structures are the C−O_2 distance (1.84 vs 1.54 Å) and the C−O−O angle (179.1 vs 112.6°). The calculated spin densities are listed in Table 4. This reaction is thermodynamically favorable with a total reaction energy of −152 kJ/mol (PCM, −160 kJ/mol). Compared to the cyclization step (path 2), the energy barrier for the reaction with O_2 (path 3) is 96 kJ/mol lower on the *hs* Fe^{III} surface, and the reaction energies are similar. Therefore, on the $S_T = 3$ spin surface, in presence of O_2, the majority of epoxide is predicted to have the oxygen atom originated from O_2, as observed experimentally.[37,100] An overview over all of the pathways to the epoxide product is given in Scheme 4.

The Reactivity of the L^1-Based Complex. Under aerobic conditions, the L^1-based catalyst yields 1 TON of oxidation products with a diol/epoxide ratio of 0.1:1 in 30 min, compared to 5 TON of epoxide exclusively in the L^2-based system; after 6 h, the yields increase to 7 and 8 TON, respectively, with the same product ratios.[37] That is, both catalysts have a similar efficiency, but the L^1-based system is much less reactive. Substantial structural differences between the two isomeric Fe^{II} catalysts with L^1 and L^2 have been observed experimentally, and the Fe^{IV} complexes have

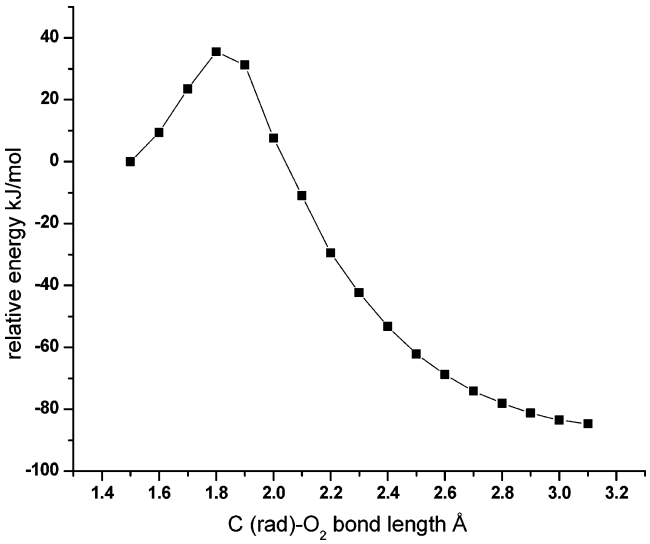

Figure 4. Potential-energy surface scan for path 3 to yield *tsIV* on the $S_T = 3$ surface. Each point represents a fully optimized geometry along the radical carbon···O_2 coordinate.

Table 4. Spin Densities of *tsIV* and *intIII* (B3LYP)[a]

spin density	Fe	O (ferryl)	C_a	C_b	O_a	O_b
tsIV $S = 4$	3.972	0.495	−0.032	0.519	0.838	1.655
intIII $S = 3$	3.966	0.496	0.015	−0.007	0.289	0.709

[a] See Figure 6 for the labels C_a, C_b, O_a, and O_b.

(99) Kolano, C.; Bucher, G.; Grote, D.; Schade, O.; Sander, W. *Photochem. Photobiol.* **2006**, *82*, 332.

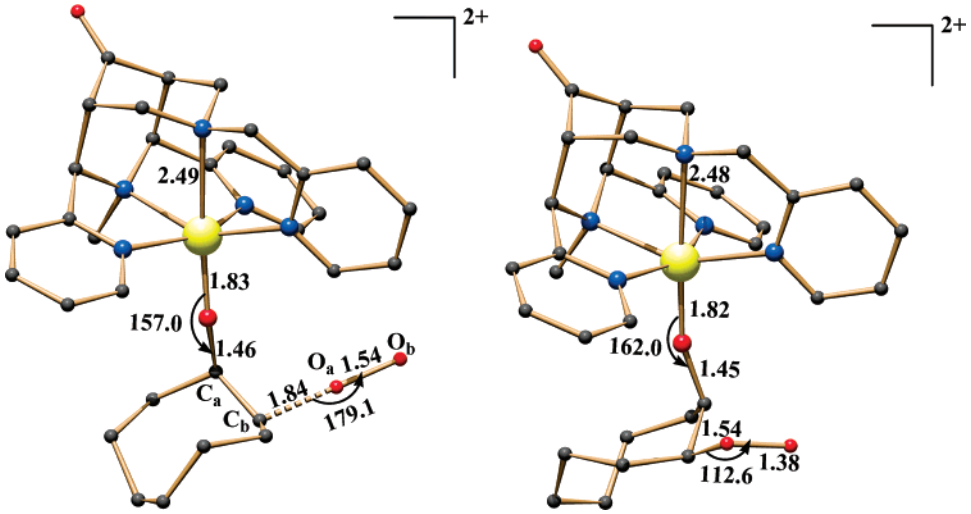

Figure 5. B3LYP-optimized structure of (a) *tsIV* and (b) *intIII* in the $S_T = 3$ configuration. All of the bond lengths are given in angstroms and angles are given in degrees.

Scheme 4

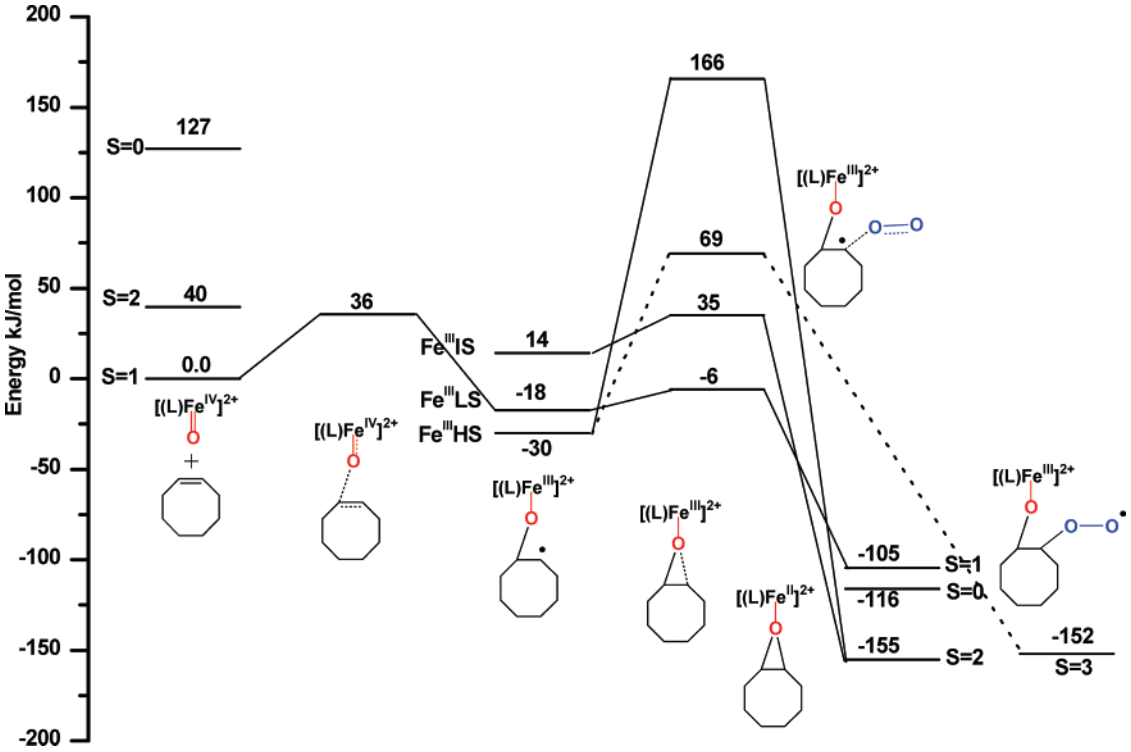

also been studied with DFT methods.[12,38,39] The metal−N3 bond distances are approximately 0.1 Å shorter than the metal−N7 distances in both complexes, and in the L^1-based system the Fe^{IV}═O bond is trans to N3, whereas it is trans to N7 in the L^2-based complex. This difference is believed to affect the efficiency of the generation of the Fe^{IV}═O species from the Fe^{II} precursors. The calculations suggest that the L^1 complex is more stable than the L^2 catalyst (above). However, the reactivity depends on the energetics of various species on the potential-energy surface. The structural data of the optimized structures of *tsII*, *intII*, and *intI* for L^1 are given in Table 1; plots of the structures are available as Figure SF7 in the Supporting Information. In *tsII*, the Fe−O bond is significantly elongated compared to the reactant (1.79 vs 1.65 Å); all of the other bonds are only slightly changed. The calculated energy barrier is 46 kJ/mol (compared to 36 kJ/mol for the more efficient L^2-based complex). The formation of *intII* is exothermic with a reaction energy of −31 kJ/mol, and this is very similar to that of the more efficient L^2-based catalyst (−36 kJ/mol). The structural parameters are also similar, except for the Fe−O−C angle, which is substantially smaller in the L^1-derived complex (157.9 vs 175.0°). However, there are significant structural differences in *intI*, where the Fe−O bond length is approximately 0.1 Å smaller than for the L^2-derivative.

(100) The transition states on the other possible spin surfaces have not been calculated. Before the formation of the product, a spin crossover occurs because the transition state and the product have different spin multiplicities.

The calculated reaction energy is −117 kJ/mol (−155 kJ/mol in the L^2-based system).

The 1,2-Dihydroxylation (Path 4). The pentadentate bispidine ligands are the only reported example of a synthetic nonheme iron model system, where a significant amount of *cis*- and *trans*-1,2-dihydroxylated products are formed.[37] Other pentadentate iron complexes produce epoxides exclusively.[3] The tetradentate ligand iron catalyst systems based on tpa and bispidines exclusively yield epoxide and *cis*-dihydroxylated products.[3,28] Extensive experimental and theoretical work with the tpa-based system was proposed to support the formation of an HO−Fe^{V}═O-type active species, which on reaction with an olefin forms a five-membered cyclic intermediate, which then cleaves to stereoselectively form cis products.[45] For the above-mentioned tetradentate bispidine system, another mechanism was proposed on the basis of a combined experimental and DFT study, and this involves an intermediate-spin Fe^{IV} dihydroxo and a high-spin Fe^{IV}-aqua-hydroxo complex.[27,28] Neither of the two proposed mechanisms is possible with pentadentate ligands.

Therefore, the diol products in the $L^{1,2}$-based systems are proposed to result from the addition of hydroxyl radicals to *intII* through *tsV*, which then yields *intIV*.[37] This is derived from experimental observations, that is, (i) no diol is produced in methanol, which is known to quench •OH radicals, (ii) no diol formation is detected under aerobic conditions, where O_2 quenches *intII*, and (iii) there is sterochemical scrambling of the dihydroxylated product, and this has also been observed with *cis*-2-heptene as the substrate.[37] The hydroxyl radicals are proposed to emerge from the homolytic cleavage of the O−O bond in Fe^{III}−OOH (Scheme 1), and they are proposed to be stabilized in a solvent cage before they are available for the hydroxylation step.[37,39] Attempts to calculate the transition state *tsV* with spin up on the carbon and on the •OH radical, or a broken symmetry type calculation with spin up on the carbon radical and spin down on the •OH radical, both on the *hs* Fe^{III} surface, collapsed to the product *intIV*. The formation of *intIV* is exothermic by −377 kJ/mol. Because this is a radical combination reaction, the barrier is very small or it is a barrierless reaction.

Theoretical work on cytochrome P450 shows that hydroxylation may proceed via the cleavage of the FeO···OH bond, producing an •OH radical in a hydrogen-bonded resting state (OH···ferryl oxygen interaction), before it attacks the substrate (so-called "Somersault mechanism").[101] On the basis of the experiments,[37] $[(L^2)FeOOH]^{2+}$ was assumed to be the source for •OH radicals, and calculations of the attack of $[Fe(L^2)OOH]^{2+}$ at *intII* were also done (Scheme 5, *tsVI*). As an alternative for the production of 1,2-diols, the direct oxidation of cyclooctene by Fe^{III}−OOH was also considered (*tsVII* in Scheme 5). For the Fe^{III}−OOH complexes, the *ls* electronic configuration ($S = {}^1/_2$) is found to be the ground state, consistent with experiments.[38,102] The *is* and *hs* spin states are 47 and 26 kJ/mol above the ground state, respectively (PCM, 53 and 36 kJ/mol). The optimized structure of the *ls* configuration is shown in Figure 6; structural parameters for all of the spin states are presented in Table 1. The transition state *tsVI* involves two iron centers (attack of $[Fe(L^2)OOH]^{2+}$ at *intII*). However, to limit the computational expense the Fe−O fragment was replaced by a hydroxyl group (Scheme 5, *tsVI*). The optimized structure of this transition state on the *ls* Fe^{III} surface is also shown in Figure 6. The energy of the transition state is 17 kJ/mol lower than the reactants, (Fe^{III}−OOH, $C_8H_{15}O$ radical). However, the transition state is preceded by a weak complex formation. This is shown in part b of Figure 6, where the hydroxyl group of the $C_8H_{15}O$ radical is hydrogen bonded to Fe^{III}−OOH. This complex is computed to be lower in energy than that of the reactant by 102 kJ/mol, and the energy barrier for the formation of *tsVI* is 85kJ/mol. The final products of this reaction are 1,2-dihydroxycyclooctane and the Fe^{IV}═O oxidant. The reaction energy is −220 kJ/mol, and the overall energetics reveal that this is a very favorable reaction channel. Note that the energy profile is significantly different with solvated molecules, that is, the barrier for the transition state is 41 kJ/mol above the reactant. Therefore, no weak complex intermediate is expected in solution. The reaction is found to be exothermic by 205 kJ/mol.

Scheme 5

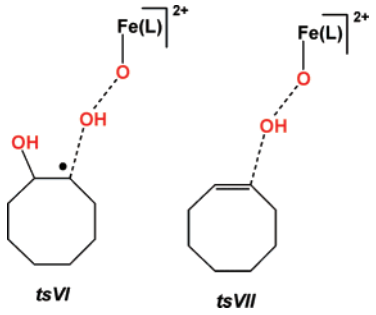

The optimized transition state *tsVII* of the alternative path of Scheme 5 on the *ls* Fe^{III} surface is also shown in Figure 6 (also Scheme 6). Here, the O−O bond is elongated, and the Fe−O−O angle is opened from 117.1 to 122.7 degrees. The computed spin densities of the Fe−OOH reactant and the transition state *tsVII* are given in Table 5. The spin density on the metal center is delocalized to the proximal and distal oxygen atoms. In the transition state, the distal oxygen gains significant negative spin density due to the elongated O−O bond and therefore has significant radical character. The calculated barrier for the oxidation is 17 kJ/mol (PCM, 71 kJ/mol), and the products of this reaction are Fe^{IV}═O and a $C_8H_{15}O$ radical, with a reaction energy of −39 kJ/mol (PCM, −5 kJ/mol).[103,104]

(101) Bach, R. D.; Dmitrenko, O. *J. Am. Chem. Soc.* **2006**, *128*, 1474.
(102) Bautz, J.; Comba, P.; Que, Jr., L. *Inorg. Chem.* **2006**, *45*, 7077.

(103) The energy of the product was obtained in a calculation, where the hydrogen atom of the hydroxyl group is hydrogen-bonded to the oxygen of the Fe^{IV}═O group.
(104) Note that the formations of *tsV* and *tsVI* are bimolecular reactions and entropy effects, which are not included, are important. The reaction involving *tsVII* is presented as barrierless in Scheme 6, and entropy effects clearly will increase the energy barrier.

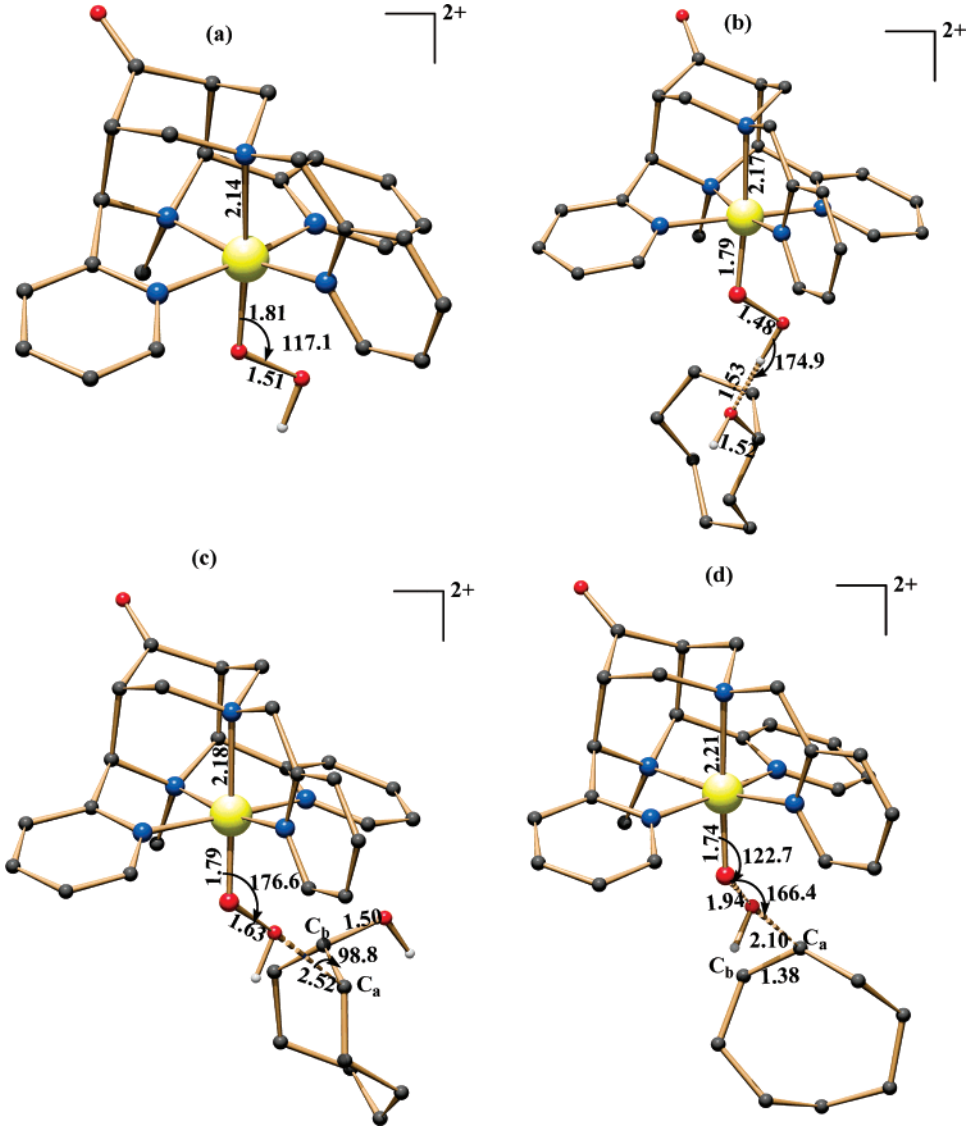

Figure 6. B3LYP-optimized structures of L^2-based complexes: (a) $Fe^{III}-OOH$ in the $S = {}^1/_2$ configuration, (b) weak complex before the formation of *tsVI*, (c) *tsVI*, (d) *tsVII*. All of the bond lengths are given in angstroms and the angles are given in degrees.

Two-State Reactivity: Participation of the $S = 2$ State in the Catalytic Mechanism. So far, only the $S = 1$ state of the $Fe^{IV}=O$ complex has been considered. The $S = 2$ state lies only 40 kJ/mol higher in energy and may also participate in the catalytic mechanism (Scheme 4). Participation of different spin states is well-documented for both heme and nonheme iron complexes. DFT studies on the mechanism of the epoxidation of ethylene by cytochrome P450 suggest the involvement of several spin states in the reaction (multistate epoxidation),[63] and two-state reactivity has been found in the hydroxylation of alkanes with different types of nonheme iron complexes.[42,43,105−108] For the reaction described here, on the $S = 1$ and $S = 2$ spin surfaces a common intermediate (*intII*) is formed after the first transition state (*tsII*). Because of difficulties to converge the correct spin state with an unrestricted wave function for the transition state on the $S = 2$ surface, a restricted open-shell calculation (ROB3LYP) was performed. To obtain an estimate of the barrier, the reactant and the radical intermediate (*intII*, $S_T = 3$) were also optimized at the same level. The stepwise transition state is preceded by a weak complex, which results in a stabilization of −17 kJ/mol compared to the reactant (Scheme 7). The calculated energy barrier for the transition state (*tsII*) is 20 kJ/mol from the weak complex (only 2 kJ/mol from the reactant), and the reaction is exothermic with a reaction energy of −39 kJ/mol. The optimized structure and structural data of the transition state are given in Figure 7 and Table 1. The O−C distance of the newly forming bond is somewhat longer on the $S = 2$ than on the $S = 1$ surface. Moreover, this structure looks more like an asynchronous concerted transition state because the distances from the ferryl oxygen to the two carbon atoms differ only by approximately 0.2 Å, unlike those of the $S = 1$ structure (1.99 and 2.63 Å). The spin densities on the olefinic carbon atoms also emphasize this point (Table 2).

(105) Cohen, S.; Kozuch, S.; Hazan, C.; Shaik, S. *J. Am. Chem. Soc.* **2006**, *128*, 11028.
(106) Derat, E.; Shaik, S. *J. Am. Chem. Soc.* **2006**, *128*, 8185.
(107) Kumar, D.; Visser, O.; Sam, P. d.; Shaik, S. *Chem.—Eur. J.* **2005**, *11*, 2825.
(108) Meunier, B.; de Visser, S. P.; Shaik, S. *Chem. Rev.* **2004**, *104*, 3947.

Scheme 6

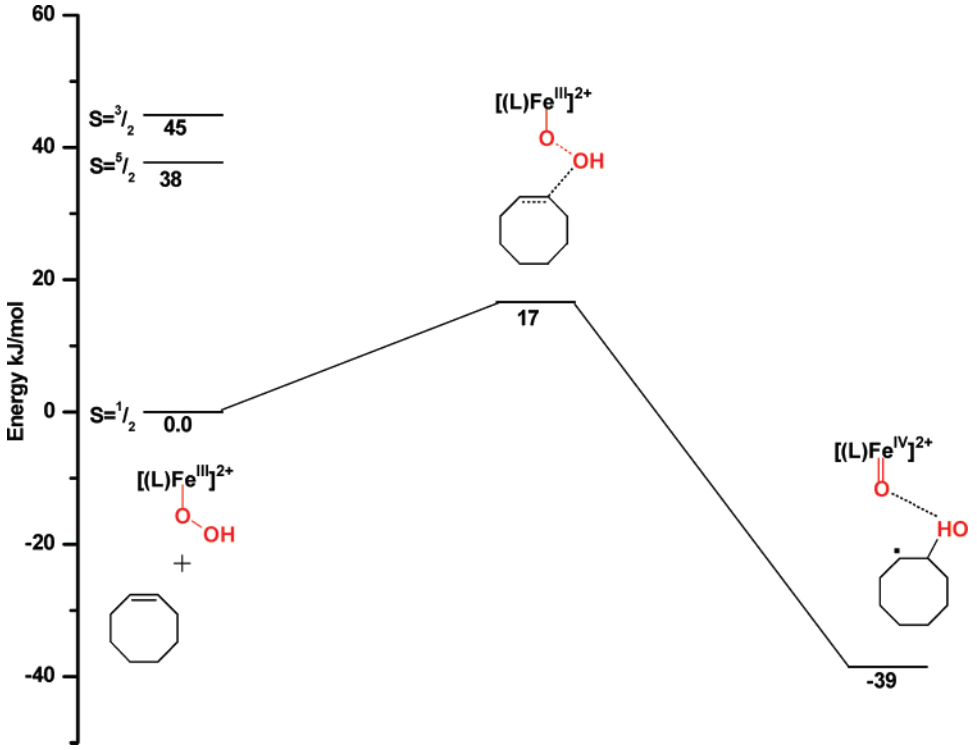

Table 5. Spin Densities of Fe^{III}−OOH and *tsVI* (B3LYP)[a]

		Fe	O (ferryl)	O	C_a	C_b
$Fe^{III}OOH$	$S = 1/2$	0.835	0.214	0.022		
	$S = 3/2$	2.736	0.084	0.015		
	$S = 5/2$	3.967	0.446	0.089		
tsVI	$S = 1$	0.821	0.465	−0.042	0.017	0.031
	$S = 1/2$	0.768	0.806	−0.218	0.809	0.002

[a] See Figure 7 for the labels C_a and C_b.

Discussion

The hybrid B3LYP functional has been shown to be viable in the prediction of the correct spin-state ordering.[63,72−75] Two species that can be directly compared with experimental data are the Fe^{IV}═O and the Fe^{III}−OOH complexes. The B3LYP functional predicts the correct spin ground state in both cases. Therefore, the majority of the calculations were performed with B3LYP, and the discussion focuses on the results from the B3LYP gas-phase calculations.

The energetics of the species discussed here are assembled in Scheme 4. The concerted mechanism for the formation of epoxide from ferryl oxygen transfer is disregarded, as no true transition state was found. It is interesting to note that the heme Fe^{IV}═O center in cytochrome P450 also undergoes a stepwise mechanism for the olefin oxidation, and there is published computational and experimental evidence for this interpretation.[63,109,110] In our nonheme iron system, the stepwise mechanism, which leads to the formation of the radical intermediate, is energetically accessible with an energy barrier of 36 kJ/mol, and this is considerably smaller than that observed in the ethylene oxidation by cytochrome P450 and the aromatic epoxidation/hydroxylation by nonheme Fe^{IV}═O complexes, where the activation energy for the formation of radical intermediates is in the range of 58−83 kJ/mol.[63,72] The oxidation state of the iron center shifts from IV to III during this reaction, and the *hs* Fe^{III} state is energetically preferred. The radical intermediate is 30 kJ/mol lower in energy than the reactant, and this is also energetically more favorable than with cytochrome P450.

On the basis of the available experimental data, a relatively long lifetime of the radical intermediate *intII* has been proposed. For this to be valid, the radical intermediate must be energetically accessible, and its decay must have significant energy barriers. The calculations confirm this scenario and show that the radical intermediate is kinetically as well as thermodynamically accessible. The barrier for the cyclization on the same surface ($S_T = 3$) is prohibitively high. However, the MECP calculation reaveals that the reaction proceeds via a spin-crossover (preferably to the *ls* but possibly to the *is* surface; both are energetically accessible) with a relatively low-energy barrier. The autoxidation to epoxide proceeds via the reaction of O_2 with the carbon-based radical intermediate. The energy barrier for this reaction on the $S_T = 3$ surface is not prohibitively high, and there is a possibility for a lower barrier on other spin surfaces but this has not been evaluated. The energy barriers for the reaction of the radical intermediate to form the product by cyclization in cytochrome P450 are generally smaller.[63,72]

A possible two-state scenario has been explored by calculations on the $S = 2$ surface of the Fe^{IV}═O complex of L^2. The energy gap between the $S = 1$ and $S = 2$ states of the ferryl cation is 40 kJ/mol and the calculated barrier for *tsII* on the $S = 1$ surface is 36 kJ/mol, whereas on the $S = 2$ surface the barrier is much smaller (2 kJ/mol from the

(109) Gross, Z. *J. Biol. Inorg. Chem.* **1996**, *1*, 368.
(110) Gross, Z.; Nimiri, S.; Brazilay, C. M.; Simkhovich, L. *J. Biol. Inorg. Chem.* **1997**, *2*, 492.

Scheme 7

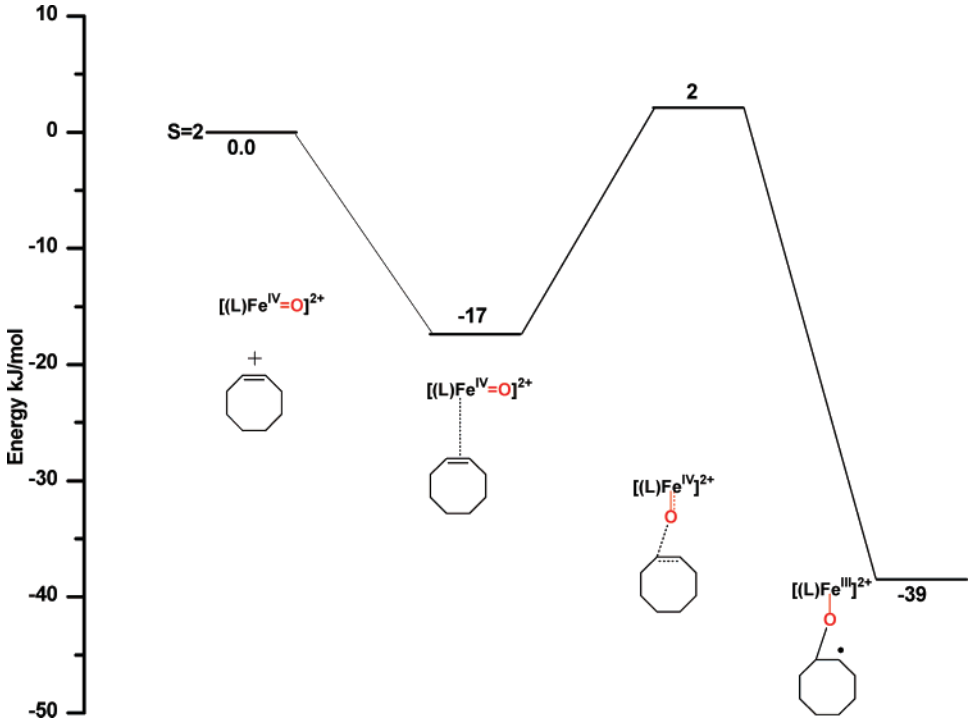

reactant at the ROB3LYP level). Therefore, it is possible that the observed reactivity is an interplay of both spin states.

An issue for which a direct comparison with experiment is available is the very different reactivity of the two catalysts based on the isomeric ligands L^1 and L^2. The two catalysts lead to the same products and therefore probably follow the same mechanism, but the L^1-based system is at least seven times less efficient.[37] The energies of the Fe^{IV}═O complexes of L^1 and L^2 differ significantly and that with L^1 is more stable by 12 kJ/mol. The calculated energy barrier to the first transition state (*tsII*) is also different for the two isomeric catalysts; the L^1-based complex has a barrier higher by approximately 10 kJ/mol. However, the stabilization of the radical intermediate is similar in both systems. The important difference, and a possible reason for the different reactivities, is the formation of *intI* (the product of the epoxidation path). A short and strong Fe−O bond in *intI* leads to a reduced substitution rate. For L^1, the Fe−O bond is approximately 0.1 Å shorter than for L^2, and the total reaction energy between the reactant and *intI* is substantially smaller for the L^1-based catalyst system (−117 vs −155 kJ/mol).

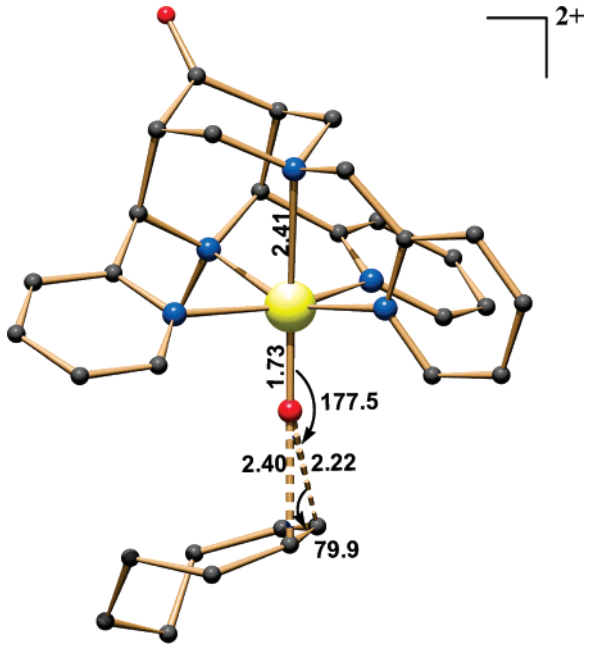

Figure 7. DFT-optimized structure of *tsII* in the $S = 2$ configuration (L^2-based system). All of the bond lengths are given in angstroms and the angles are given in degrees.

Of particular interest is the 1,2-dihydroxylation of olefins with the L^1- and L^2-based catalysts.[37] Pentadentate ligand nonheme iron model compounds generally produce exclusively epoxides, and the tetradentate tpa-based catalysts yield exclusively cis diols.[3] In sharp contrast, the pentadentate bispidine-based iron catalysts yield cis and trans diols, both with cyclooctene and *cis*-2-heptene substrates.[37] Two possible mechanisms have been evaluated by DFT. The reaction of a hydroxyl radical with *intII* to form *intIV* is thermodynamically favorable with an exceedingly low-energy barrier. The formation of the diol product from *intIV* requires the cleavage of an Fe−O bond, and this is assumed to be the rate-limiting step in this reaction. The second possibility is the formation of a diol product from Fe^{III}−OOH (Scheme 6). Starting with Fe^{III}−OOH, two different reactions have been studied, one, where the hydroperoxo complex is the source of the hydroxyl radical and the other, where it directly oxidizes the olefin. The reaction of *intII* with Fe^{III}−OOH is barrierless in the gas phase (*tsVI*). However, this also requires the cleavage of the Fe−O bond of *intII* to yield the diol product, and this step might be rate limiting. The direct oxidation of cyclooctene by Fe^{III}−OOH to form the diol product has a very

low energy barrier, and this reaction is in agreement with the experiments[37] because Fe^{IV}═O selectively oxidizes cyclooctene to epoxide products. The first energy barrier for the direct oxidation by the hydroperoxo complex is small, relative to the epoxidation by the Fe^{IV}═O oxidant, and, therefore, the formation of diols by this mechanism cannot be excluded.

Conclusions

DFT (B3LYP) calculations of the epoxidation and 1,2-dihydroxylation of olefins with the bispidine/iron(II)/H_2O_2 catalyst systems fully support the mechanism proposed by experiment. The main feature is the formation of a common radical intermediate, which may undergo cyclization or react with O_2 to yield epoxide, or react with an •OH radical to form diol products. Both pathways for the epoxide formation are energetically accessible, and the DFT calculations predict a spin-crossover in the ferryl oxygen transfer path. On the basis of the calculated energy barriers and energetics of the reaction, the experimentally determined product distribution (epoxide, cis and trans diols) and isotopic labeling data can be rationalized.[37] Alternative routes for the dihydroxylation were also investigated, and the computations show that the direct oxidation of olefins by Fe^{III}−OOH has a low-energy barrier. The study suggests a possible two-state scenario, where $S = 1$ and $S = 2$ states participate in the catalytic cycle.

Acknowledgment. Financial support by the German Science Foundation (DFG) and an AvH fellowship to G.R. are gratefully acknowledged.

Supporting Information Available: A discussion of the singlet state of the Fe^{IV}═O complexes, the search for the concerted transition state *tsI*, the optimized structures and MOs of the L^1-based complexes, imaginary frequencies for the reported transition states and a table with the computed total energies of the species discussed here together with the $\langle S^2 \rangle$ values. This material is available free of charge via the Internet at http://pubs.acs.org.

IC701161R